

Large-scale extreme rainfall producing synoptic systems of the Indian summer monsoon

Akshaya C Nikumbh¹, Arindam Chakraborty², G S Bhat², and Dargan M. W. Frierson³

¹Indian Institute of Science Bangalore

²Indian Institute of Science

³University of Washington

November 21, 2022

Abstract

In recent years India has been increasingly experiencing widespread floods induced by large-scale Extreme Rainfall Events (LEREs). LEREs are mainly associated with monsoon Low-Pressure Systems (LPS). The forecast of these high-flood-potential events, however, has remained challenging. Here, we compare LPSs of the summer monsoon that led to LEREs (LPS-Lg) and strong LPSs that did not result in LEREs (LPS-noLg) over central India for the period 1979-2012. We show that having a strong LPS is not a sufficient condition to produce LEREs, and the LPS-Lg are accompanied by Secondary Cyclonic Vortices (SCVs). The simultaneous existence of LPS and SCV creates a giant mid-tropospheric vortex. SCVs enhance dynamic lifting, static instability, and moisture transport from the Arabian Sea that precondition the atmosphere for deep convection. SCVs also slow down the propagation of LPSs. We show that the interaction of synoptic-scale systems can lead to LEREs even if individual systems aren't strong enough.

1 **Large-scale extreme rainfall producing synoptic systems**
2 **of the Indian summer monsoon**

3 **Akshaya C. Nikumbh^{1,2,3}, Arindam Chakraborty^{1,2}, G.S. Bhat^{1,2}, Dargan M.**
4 **W. Frierson³**

5 ¹Centre for Atmospheric and Oceanic Sciences, Indian Institute of Science, Bangalore, 560012, India.

6 ²Divecha Centre for Climate Change, Indian Institute of Science, Bangalore, 560012, India.

7 ³Dept. of Atmospheric Sciences, University of Washington, Seattle, 98195, USA.

8 **Key Points:**

- 9
- 10 • A mechanism for large-scale extreme rainfall events of central India is proposed.
 - 11 • Large-scale extreme rainfall events occur when monsoon low pressure systems are
12 assisted by secondary cyclonic vortices.
 - 13 • The interaction of two cyclonic vortices form conditions favourable for long-lived,
organized, and slow moving convective systems.

Corresponding author: Akshaya C. Nikumbh, nikumbh@iisc.ac.in

Abstract

In recent years India has been increasingly experiencing widespread floods induced by large-scale Extreme Rainfall Events (LEREs). LEREs are mainly associated with monsoon Low-Pressure Systems (LPS). The forecast of these high-flood-potential events, however, has remained challenging. Here, we compare LPSs of the summer monsoon that led to LEREs (LPS-Lg) and strong LPSs that did not result in LEREs (LPS-noLg) over central India for the period 1979-2012. We show that having a strong LPS is not a sufficient condition to produce LEREs, and the LPS-Lg are accompanied by Secondary Cyclonic Vortices (SCVs). The simultaneous existence of an LPS and an SCV creates a giant mid-tropospheric vortex. SCVs enhance dynamic lifting, static instability, and moisture transport from the Arabian Sea that precondition the atmosphere for deep convection. SCVs also slow down the propagation of LPSs. We show that the interaction of synoptic-scale systems can lead to LEREs even if individual systems are not strong enough.

Plain Language Summary

Over the past two decades, India has endured many widespread floods caused by large-scale heavy rainfall events during the monsoon season that resulted in huge losses to life and property. The large-scale heavy rainfall events, though rare, have become more frequent recently. We show that these events occur when multiple monsoon low pressure systems are present at the same time. While the individual systems themselves need not be very strong, their simultaneous presence makes the environment conducive for sustained and organized deep convection, leading to large-scale heavy rainfall events over central India.

1 Introduction

Understanding the physical processes that lead to extreme rainfall events (EREs) is a challenging multiscale problem that has received wide attention in the literature. The literature on EREs includes aspects like flash floods (Maddox et al., 1978, 1979; Bosart & Sanders, 1981), convective systems (Doswell III et al., 1996; Schumacher & Johnson, 2005), the observed trends (B. N. Goswami et al., 2006; Rajeevan et al., 2008; Karmakar et al., 2017; Nikumbh et al., 2019), and their future projections (Trenberth, 1999; Emori & Brown, 2005; Muller et al., 2011; O’Gorman, 2015). A multitude of extreme precipitation events, however, remained unpredicted (Coumou & Rahmstorf, 2012). Predicting the location and intensity of extreme precipitation, and avoiding false alarms continue to be major challenges in weather forecasting. Though EREs have different features based on their time and location, there are certain common characteristics that can be used for their forecasting. The ingredients for extreme precipitation include moist ascent, static instability, dynamic lifting and moisture supply (Doswell III et al., 1996). These ingredients are often brought together in the presence of synoptic systems and hence EREs are often associated with synoptic systems.

During the Indian summer monsoon season, a large part of kinetic energy at mid levels is contributed by synoptic systems such as Low Pressure Systems (LPSs) and Mid-Tropospheric Cyclones (MTCs) that form over the surrounding ocean and the Indian subcontinent (Krishnamurti & Hawkins, 1970). LPSs form most frequently over the Bay of Bengal (BoB) and move north-westward over the Indian subcontinent (Sikka, 1978; Godbole, 1977). They contribute around half of the rainfall over the core monsoon zone (Hunt & Fletcher, 2019; Sikka, 1977) and often lead to heavy rainfall events over central India (Ajayamohan et al., 2010). The southwestern sector of LPSs is known to receive heavy rainfall, often exceeding 300 mm day^{-1} (Godbole, 1977; Krishnamurthy & Ajayamohan, 2010). In the past two decades, India has experienced many devastating floods triggered by extreme rainfall viz., the Kerala flood of August 2018 (Baisya & Pattnaik, 2019), Chennai flood of Dec 2015 (Phadtare, 2018; Chakraborty, 2016), Uttarakhand flood of June 2013 (Houze Jr et al., 2017), Leh flood of June 2010 (Rasmussen & Houze Jr, 2012), and Mumbai

64 flood of July 2005 (Kumar et al., 2008). Though each individual event had unique features,
 65 the common thread in all events was the presence of an LPS. In every season around 15 to 18
 66 LPSs are observed (Figure 1a) and almost two-third produce at least one ERE over central
 67 India and remaining 33% do not give extreme rainfall. A comprehensive understanding of
 68 the conditions that stimulate LPSs to produce EREs is missing. To address the problem of
 69 false alarms it is important to understand the conditions under which LPSs are more likely
 70 to give rainfall extremes.

71 EREs over the west coast of India are often associated with synoptic systems such as
 72 MTCs, off-shore troughs, and vortices (Francis & Gadgil, 2006; Pradhan et al., 2015; Carr,
 73 1977). An active offshore trough (Wang, 2006) and mesoscale vortices (George, 1956) often
 74 lead to heavy rainfall reaching over 300 mm day^{-1} to 500 mm day^{-1} near the west coast
 75 (Wang, 2006). Past studies have extensively examined the influence of MTCs and offshore
 76 trough/vortices on heavy rainfall events over the western states (Miller & Keshavamurthy,
 77 1968; Francis & Gadgil, 2006; Pradhan et al., 2015; Carr, 1977). However, the possibility of
 78 synoptic systems of the west coast influencing heavy rainfall events further eastward, over
 79 central or eastern Indian states has not been explored yet.

80 It has been observed that the Large-scale Extreme Rainfall Events (LEREs, area \geq
 81 $70 \times 10^3 \text{ km}^2$) over central India are increasing significantly (Nikumbh et al., 2019). The
 82 LEREs are of a great concern as they are more likely to cause widespread flooding compared
 83 to small-scale scattered events. For example, the recent flood over India in the first week of
 84 August 2019 (Carlowicz, 2019), Kerala flood of mid-August 2018 (Baisya & Pattnaik, 2019),
 85 Gujarat flood of July 2017 (Thiruppugazh, 2019) were caused by the widespread extreme
 86 rainfall events that spanned over the entire state and resulted in hundreds of deaths. This
 87 underscores the urgency of improving an understanding of the physical process that lead
 88 to LEREs. The LEREs of the Indian summer monsoon are predominantly associated with
 89 monsoon LPSs (Nikumbh et al., 2019). During the monsoon season there is a high chance
 90 (probability=0.66) of getting an ERE over central India given an LPS, however, probability
 91 of getting an LERE is extremely rare (probability=0.04) (Figure 1a). This poses some
 92 interesting questions: why do so few LPSs result in LEREs? Are LEREs associated with
 93 some of the strongest and rare LPSs? In this study we pursue these questions by comparing
 94 characteristics of LPSs and meteorological conditions that lead to LEREs (LPS-Lg) and
 95 strong LPSs (intensity ≥ 2) that did not result in LEREs (LPS-noLg).

96 2 Datasets and methods

97 We use the daily $1^\circ \times 1^\circ$ gridded rainfall dataset prepared by the India Meteorological
 98 Department (IMD) (Rajeevan et al., 2006) for the monsoon months (June to September) of
 99 the period 1979 to 2012. The EREs are defined following the same procedure as in Nikumbh
 100 et al. (2019). The 99.5th threshold is used to define extreme rainfall at each grid and then
 101 the neighbouring grids with simultaneous extreme precipitation are combined using the
 102 connected component labelling algorithm (Falcão et al., 2004). The EREs that span over
 103 an area more than five $1^\circ \times 1^\circ$ grids (area $\geq 70 \times 10^3 \text{ km}^2$) are defined as LEREs. Then
 104 we iteratively check the consecutive days of EREs to find if there is an overlap over at least
 105 one grid cell of the location of EREs. If an overlap in the locations of EREs exist for the
 106 consecutive days, only the first day of the largest EREs is considered for the calculation.
 107 This makes sure that the same event is not counted again. Over the Indian subcontinent,
 108 the LEREs occur mainly between 15° to 25°N (Nikumbh et al., 2019) and we select this
 109 region ($15^\circ\text{-}25^\circ\text{N}$, $65^\circ\text{-}85^\circ\text{E}$) as our study area (boundaries shown in Figure 1b). Over the
 110 study region 24 such LEREs were observed from 1979 to 2012.

111 The dataset by Hurley and Boos (2015) is used for LPSs. This dataset identifies
 112 LPSs using ERA-Interim 850 hPa relative vorticity. They applied an automated tracking
 113 algorithm (Hodges, 1995, 1999) on a 6-hourly 850 hPa relative vorticity field. The tracking
 114 algorithm is based on the optimization of the cost function for motion (Hodges, 1999). It

115 is used to identify relative vorticity maxima (or minima in the southern hemisphere) and
 116 to track its path. Only those vortices are considered whose maxima (or minima) exceeds
 117 a magnitude of $0.5 \times 10^{-5} \text{ s}^{-1}$. Additional filtering criteria includes that the LPS should
 118 last for two or more days and should have at least one point of the track is in the monsoon
 119 region. They use additional criteria of the mean sea-level pressure anomaly and surface
 120 wind speed (10 m) to define the intensity of LPS. The intensities 1 and 2 correspond to
 121 monsoon lows (pressure anomaly ≥ 2 hPa) and depressions (pressure anomaly between 4
 122 to 10 hPa and wind speed between $8.5 \frac{\text{m}}{\text{s}}$ and $13.5 \frac{\text{m}}{\text{s}}$) respectively. Intensity 3 indicates
 123 deep depression and above (pressure anomaly ≥ 10 hPa and wind speed $\geq 13.5 \frac{\text{m}}{\text{s}}$). The
 124 presence of LPSs is checked for each LERE within the domain of 10° - 30° N, 65° - 85° E (LPS
 125 domain). Out of 24 LEREs, 22 had the presence of LPSs. We compare these 22 LPSs that
 126 led to LEREs (LPS-Lg) and 132 strong LPSs (intensity ≥ 2) that passed through the LPS
 127 domain but did not cause LEREs (LPS-noLg). For the meteorological variables, the daily
 128 data from the ECMWF interim reanalysis (ERA-Interim; (Dee et al., 2011)) is used, at the
 129 spatial resolution of $1^\circ \times 1^\circ$.

130 Secondary Cyclonic Vortices (SCVs) to the west of LPSs are confirmed by relative
 131 vorticity maps (Figure S1, Figure S2). The type of weather systems associated with SCVs are
 132 verified using the IMD weather reports. The SCVs are reported either as cyclonic circulation
 133 or monsoon lows in the IMD weather report (details in supplementary information).

134 **3 Results and discussions**

135 **3.1 LPSs and extreme rainfall events**

136 The average number of LPSs observed over the study region per season is 15. Around
 137 66% of LPSs during the study period were associated with at least one ERE over the
 138 study region. Though the number of LPSs that results in EREs varies from year to year
 139 (Figure 1a), there is not a single year when LPSs of the monsoon season did not cause any
 140 ERE over central India. This supports the idea of a strong association between EREs over
 141 central India and LPSs. On the other hand, there are 2 to 5 LPSs in a season that pass
 142 through central India without causing any EREs, thus underscore the uncertainty tied to
 143 this association between LPSs and EREs.

144 The relative vorticity distribution (Figure S3) for the two types of LPSs show that
 145 the LPS-Lg have a higher median vorticity ($7 \times 10^{-5} \text{ s}^{-1}$) than LPS-noLg ($6 \times 10^{-5} \text{ s}^{-1}$).
 146 However, there are many LPSs in LPS-noLg that had higher relative vorticity than LPS-Lg.
 147 During the study period, out of the 9 strongest LPSs (with intensity ≥ 3) only 3 led to
 148 LEREs. On the other hand, 82% of LEREs were associated with LPSs with intensity ≥ 2 .
 149 This suggests that the LPSs that lead to the LEREs tend to be stronger, but their strength
 150 is not a sufficient condition to get LEREs.

151 **3.2 Large-scale extreme rainfall events**

152 The LEREs show a peculiar geographical preference. They occur mainly over the
 153 zonal belt in between the frequent locations of synoptic systems of the east and west coast
 154 (Figure 1b). The mean seasonal climatology of geopotential height at mid-levels captures
 155 these two frequent locations of synoptic systems that have centers around $\sim 84^\circ$ E and
 156 $\sim 72^\circ$ E (Karmakar et al., 2015). As LPSs of the east coast are more frequent, the eastern
 157 location is better defined with sharper gradients than the west. Note that both of these
 158 centers are present around the same latitudinal belt ($18^\circ - 20^\circ$ N) with the west center
 159 being slightly southward ($\sim 18^\circ$ N). Consequently, there are two locations where the LEREs
 160 occur most frequently, one near the east coast ($\sim 80^\circ$ E) and the other near the west coast
 161 ($\sim 76^\circ$ E). The climatological surface monsoon trough (Y. Rao, 1976) and low-level jet (LLJ,
 162 shown in Figure S4) (Findlater, 1969; Joseph & Sijikumar, 2004) lie on the northern and
 163 southern side of LEREs, respectively.

164 The LEREs occur in the southwestern sector of LPSs (Nikumbh et al., 2019). We
 165 observe that the LPS-Lg are accompanied by SCVs on their western flank (Figure S1). Of
 166 all the SCVs that occurred with LPS-Lg, 57% were identified as cyclonic circulation and
 167 24% as monsoon lows in the IMD weather reports. The cyclonic circulation includes the
 168 lower- or mid-tropospheric systems, and the monsoon lows refers to the lows, depressions
 169 and cyclonic storms. 19% of SCVs were not identified as weather systems by the IMD,
 170 however, the presence of a vortex (vorticity $\geq 2 \times 10^{-5} \text{ s}^{-1}$ at 500 hPa and 850 hPa) has
 171 been manually verified using the vorticity map (Figure S1, Figure S2).

172 There are two frequent genesis regions for LPS-Lg over the BoB, one at 20°N and the
 173 other at 15°N (Figure 1c). The LPS-Lg tracks are southward compared to LPS-noLg. The
 174 LPS-Lg show a westward extension of LPSs tracks. The LPS-noLg have a shorter path and
 175 their genesis locations are mainly observed in the north BoB ($\sim 20^\circ\text{N}$) (Figure 1d). As the
 176 LPSs on the southern side are more likely to encounter the effect of synoptic systems of the
 177 west coast (Figure 1c), the genesis location and track density of LPS-Lg paths show a peak
 178 on the southern side ($\sim 15^\circ\text{N}$). The westward extension of the path of LPS-Lg possibly
 179 indicates a long lifetime of LPS-Lg. In the next sections, we examine how the interaction
 180 between LPSs and SCVs lead to LEREs.

181 3.3 Mid-tropospheric vortex, dynamic lifting and organized convergence

182 Two days before the LEREs, the presence of both an LPS over the BoB and an SCV over
 183 the west coast is evident at 500 hPa (Figure 2a). The LPS continues to move westward and
 184 the circulations associated with both vortices merge a day before the event. This leads to the
 185 formation of a giant mid-tropospheric cyclonic vortex (MCV) over central India. An MCV
 186 is often observed in long-lived mesoscale convective systems (MCSs) (Bartels & Maddox,
 187 1991; Fritsch et al., 1994; Bartels et al., 1997). A vorticity budget analysis suggests that it
 188 forms by advection of vorticity from the environment and generation of vorticity by MCSs
 189 themselves (Knievel & Johnson, 2002, 2003). MCSs that develop a stratiform region perturb
 190 the vertical temperature gradient and tends to concentrate positive potential vorticity at
 191 midlevel, which manifests as a midlevel vortex (Raymond & Jiang, 1990). The MCV in turn
 192 promotes new convection and extends the lifetime of MCSs (Fritsch et al., 1994; Raymond
 193 & Jiang, 1990). MCVs also help in organizing the deep convection (Schumacher & Johnson,
 194 2009). The mid-level vortex generated by interaction of LPS and SCV thus could help in
 195 forming long-lived organized convection conducive for widespread extreme rainfall.

196 Strong ascent associated with the LPS and a comparatively weaker SCV ascent are
 197 apparent in the vertical structure of pressure velocity (ω) (Figure 2b). Rising motion
 198 is observed on the west and sinking motion on the east of cyclonic vortices, as observed in
 199 earlier studies (Krishnamurti & Hawkins, 1970; Sikka, 1978). Both SCV and LPS exist in
 200 an easterly sheared environment owing to reversal of the meridional temperature gradient.
 201 The interaction of these vortices with easterly shear produces the maximum ascent on the
 202 western side (K. Rao & Rajamani, 1970; Sanders, 1984). This can be simply shown by
 203 using an approximate form of the quasi-geostrophic equation (Sutcliffe, 1947; Trenberth,
 204 1978; Boos et al., 2015)

$$\Delta w \sim f_o \frac{\partial u_g}{\partial p} \cdot \nabla(2\xi_g + f) \quad (1)$$

205 Where, Δ -Laplacian operator, w -pressure velocity, f and f_o are the Coriolis parameter and
 206 the mean Coriolis parameter, respectively, and u_g and ξ_g are the geostrophic wind and its
 207 relative vorticity, respectively. The right-hand side of Eq. (1) gives the dynamic generation
 208 of rising motion downshear of a vorticity maximum. The temperature distribution and warm
 209 advection also contribute to ascent on the western side of these systems (Krishnamurti &
 210 Hawkins, 1970; Adames & Ming, 2018a, 2018b).

211 The ascent of the SCV is horizontally narrow, vertically not that deep and stays al-
 212 most at the same location (from day-2 to day-0). The westward moving LPS has a larger

213 spatial extent and is deeper too. The orographic flow (leeward subsidence) associated with
 214 the Western Ghats is possibly preventing the low level connection between the two (Fig-
 215 ure 2b). There is also a location of ascent at the junction of LPS and SCV, resulting from
 216 the convergence at the meeting point of two systems. At day-0, the ascents merge and form
 217 a spatially large ascending region. It has been observed that the long-lived cloud systems
 218 are preferentially triggered on the western flank of LPSs, where a steep gradient of low level
 219 vorticity and temperature is present (Phadtare & Bhat, 2019). The gradients in vorticity
 220 and temperature help in setting up the rising motion (e.g., using QG omega equation) that
 221 results in forming a favourable region for long-lived cloud systems on the western flank of
 222 LPSs. The large long-lived clouds systems occur on the western flank of LPSs mainly in
 223 the band of $15^\circ - 25^\circ$ N (Figure 11 of Phadtare and Bhat (2019)), which coincides with
 224 the location of LEREs of our study. It should also be noted that the adiabatic lifting is not
 225 sufficient to explain the deep convective systems on the western flank of LPSs (Adames
 226 & Ming, 2018b, 2018a; Boos et al., 2015) and other processes that include moist thermo-
 227 dynamics also add ascent. The moist thermodynamic processes are explored in the section
 228 3.4.

229 Two days prior to the event, a low-level convergence zone forms on the western side
 230 of LPSs, and the north eastern side of SCV (Figure 2c). A day before the event two
 231 convergence zone strengthen as the LPS moves westward. On the day of the event both of
 232 them merge and form a large-scale organized convergence zone that has northwest-southeast
 233 orientation. This convergence zone could in turn support the organized convective systems,
 234 leading to widespread EREs. Only the southern part of this convergence zone experiences
 235 the LEREs.

236 3.4 Thermodynamic instability and moisture supply

237 The presence of an SCV provides moist thermodynamic instabilities that play a major
 238 role in enhancing the rainfall intensity. Figure 3a shows the vertical cross section of dry static
 239 stability, namely, Brunt Vaisala frequency ($N = \frac{g}{\theta} \frac{d\theta}{dz}$). Two days before the event, centers
 240 of static instabilities exist at midlevel over central India that are generated by convective
 241 heating associated with SCV and LPS. These instabilities merge a day before the event and
 242 the anomalies associated with the LPSs intensify even at lower levels. On the day of the
 243 event, these instabilities intensify throughout the column up to 250 hPa over central India
 244 forming a favourable environment for deep convection.

245 To examine the effects of moisture, we compare the vertical profiles of potential temper-
 246 ature (θ) and equivalent potential temperature (θ_e) (Figure S5). The moisture supply by the
 247 LLJ at low levels is evident since day-2 and it peaks on the day of the event. At day-2, the
 248 vertical profiles of θ and θ_e are similar at upper levels, indicating that moisture effects are
 249 small there. At day -1, the θ_e deviates slightly from that of θ at mid-levels as the moisture
 250 flux increases. On the day of the event, θ and θ_e profiles substantially deviate, indicating a
 251 strong moistening throughout the column. Moisture plays an important role in the growth
 252 and sustenance of LPSs (Adames & Ming, 2018a). Using a linear framework, Adames
 253 and Ming (2018b) studied the relative importance of dry and moist processes in growth and
 254 propagation of LPSs. They found that moist processes play a major role in the growth of
 255 LPSs. It should be noted that their analysis does not consider the strong background flow
 256 and vertical shear that occur during the monsoon. However, it is useful to infer that LPSs
 257 could grow just by moist processes (moisture and temperature advection and high humidity)
 258 and even without barotropic or baroclinic instabilities. The moisture supply at midlevels
 259 has been shown to enhance the vertical development in tropical convection (Bretherton et
 260 al., 2004; Holloway & Neelin, 2009). Free tropospheric moisture plays a significant role in
 261 relation between column water vapor and the transition to sustained deep convection in the
 262 tropics (Holloway & Neelin, 2009). High moisture in the free atmosphere results in higher
 263 plume buoyancies and forms conditions favorable for deep convection. The SCVs provide

264 deep inflow of moisture flux, which helps in sustaining convection in the southwestern sector
 265 of LPSs.

266 The moisture budget can be analysed by moisture transport and convergence. The
 267 column integrated moisture transport (MT) is given by,

$$MT = \frac{1}{g} \int_{P_a}^{P_s} q \mathbf{V} dp \quad (2)$$

268 Where, P_s and P_a are surface and top of atmosphere pressure respectively, g - grav-
 269 itational acceleration, q -specific humidity, \mathbf{V} -horizontal velocity. The vertical integral of
 270 moisture flux divergence (VMFD) is obtained by taking time-integral of the horizontal di-
 271 vergence of equation 2. In this study, we use the VMFD output from ERA-Interim, which
 272 was calculated by the reanalysis model.

273 The Figure 3b-c show the VMFD (shading) and MT (vectors) for LPS-Lg and LPS-
 274 noLg. In case of LPS-Lg, three main locations of moisture convergence are observed. One
 275 is to the southwest of the SCV, while the second is on the western side of the LPS and the
 276 third is to the north of LPSs center. The moisture convergence on the southwest of SCV
 277 results from the interaction of an SCV with the moisture flux by LLJ. The region of moisture
 278 convergence in the western sector of LPSs results from interaction of LPSs circulation with
 279 LLJ. Note that the westerly circulation on the southern flank of SCV enhances the strength
 280 of LLJ and in turn the moisture transport from the Arabian Sea. The eastern center forms
 281 by easterly moisture flux by the northern branch of LPSs. Since the moisture supply is
 282 mainly in the southern part of the organized convergence zone (Figure 2c), it experiences
 283 LEREs, while the northern part of convergence zone misses them (Figure S6). In case of
 284 LPS-noLg, the west coast moisture convergence zone is absent and the supply of moisture
 285 by both the Arabian Sea and the BoB is less compared to LEREs. The above analysis
 286 reveals that the moisture transport from the Arabian Sea to central India increases in the
 287 presence of an SCV.

288 3.5 Propagation speed of LPSs

289 The average propagation speed of LPSs observed during the study period is 5 m s^{-1} . In
 290 earlier studies, the propagation speed of MDs is reported as $5^\circ \text{ longitude day}^{-1}$, i.e. 6 m s^{-1}
 291 (Krishnamurti et al., 1975). From the distribution of velocity, it is clear that LPS-Lg tend
 292 to be slightly slower than the LPS-noLg (Figure S7). Around 67% of LPS-Lg have velocities
 293 lower than the average velocity ($< 5 \text{ m s}^{-1}$) along their track. The CDFs of velocities of
 294 LPS-Lg and LPS-noLg differ significantly using the KS test ($p\text{-value} < 0.06$). The speed of
 295 convective system affects the rainfall duration and in turn the accumulation of rainfall over
 296 the location (Doswell III et al., 1996). It is often observed that slower convective systems
 297 are more likely to give extreme precipitation (Maddox et al., 1978; Doswell III et al., 1996;
 298 Schumacher & Johnson, 2009). The presence of the SCV hinders the westward propagation
 299 of LPS, which results in increased accumulation of rainfall at the same place.

300 4 Summary

301 This analysis reveals that it is not only the intensity of LPSs but also the presence of
 302 SCV that determines whether LPSs could lead to LEREs. Over India, the latitudinal belt
 303 of $15^\circ - 25^\circ \text{ N}$ is the most favourable zone for the LEREs to occur. This region has frequent
 304 occurrences of synoptic systems on the western and eastern sides of mainland India. It is also
 305 accompanied by the LLJ and climatological monsoon trough on the southern and northern
 306 flanks respectively. This unique meteorological setting forms a favourable environment for
 307 LEREs. The simultaneous presence of an SCV helps an LPS by the following means to give
 308 an LERE (Figure 4).

309 **1. Mid-tropospheric vortex:** The interaction of the SCV and LPS circulation form
 310 a mid-tropospheric vortex, which is known to enhance the lifetime of MCSs and organize
 311 the convection.

312 **2. Dynamic lifting:** The presence of an SCV increases the area of dynamic lifting on
 313 the western flank of the LPSs and leads to widespread ascent at mid levels.

314 **3. Static instability:** Convection associated with the SCV provides additional static
 315 instability that could enhance the intensity of these events.

316 **4. Moisture supply:** The SCV enhances the deep layer moisture supply from the
 317 Arabian Sea that helps in sustaining deep convection.

318 **5. Organization at low-level:** Large-scale low level organized convergence forms in
 319 the region between the SCV and LPS.

320 **6. LPS translation speed:** The presence of the SCV on the western flank of the LPS
 321 slows down its westward propagation speed, which results in more accumulation of rainfall
 322 at the same location.

323 These factors provide favourable conditions to form long-lived, organized, slow moving
 324 convective systems that lead to LEREs. Our analysis could prove useful to understand
 325 the rising trend of precipitation extremes over central India, which has remained a puzzle.
 326 It gives a hint for how it is possible to get an increasing trend of LEREs in spite of an
 327 observed decreasing trend in stronger LPSs (Dash et al., 2004; Vishnu et al., 2016). We
 328 give an example of how synoptic systems could remotely influence EREs. For example,
 329 we show that synoptic systems of the west coast of India (MTCs or LPSs) can influence
 330 rainfall extremes over central and eastern states of India. Previous studies have noted the
 331 temporal and spatial clustering of synoptic activity during the active phase of monsoon
 332 (B. Goswami et al., 2003; Murakami et al., 1984). So, the predictability of LEREs could be
 333 pursued further by exploring the modulation of synoptic systems by monsoon intraseasonal
 334 oscillations, tropical waves, and Madden Julian oscillation. We recommend that a combined
 335 index that considers the simultaneous presence of multiple synoptic systems would prove
 336 more useful in the forecasting of widespread heavy rainfall events.

337 Acknowledgement

338 AC and GSB acknowledge funding from the DST, MoES and MoEF, Government
 339 of India. DMWF is supported by NSF grant AGS-1665247. ACN acknowledge support
 340 from MHRD, USIEF, India and IIE grant E0610103. This work benefited from discus-
 341 sions with Prof. M. Wallace, C. Jalihal, S. Paleri, P. Kushwah and Dr. J. Phadatare.
 342 We thank Prof. Christian Dominguez-Sarmiento and an anonymous reviewer for their use-
 343 ful comments. The rainfall data used in the study is obtained from the IMD ([http://
 344 imdpune.gov.in/ndc_new/Request.html](http://imd pune.gov.in/ndc_new/Request.html)). The global monsoon low pressure systems track
 345 dataset is available at [http://worldmonsoons.org/global-monsoon-disturbance-track-
 346 dataset/](http://worldmonsoons.org/global-monsoon-disturbance-track-dataset/). The ERA-interim dataset is available at [https://apps.ecmwf.int/datasets/
 347 data/interim-full-daily/](https://apps.ecmwf.int/datasets/data/interim-full-daily/).

348 References

- 349 Adames, Á. F., & Ming, Y. (2018a). Interactions between water vapor and potential vorticity
 350 in synoptic-scale monsoonal disturbances: moisture vortex instability. *Journal of the
 351 Atmospheric Sciences*, 75(6), 2083–2106.
- 352 Adames, Á. F., & Ming, Y. (2018b). Moisture and moist static energy budgets of south asian
 353 monsoon low pressure systems in gfdl am4. 0. *Journal of the Atmospheric Sciences*,
 354 75(6), 2107–2123.
- 355 Ajayamohan, R., Merryfield, W. J., & Kharin, V. V. (2010). Increasing trend of synoptic

- 356 activity and its relationship with extreme rain events over central india. *Journal of*
 357 *Climate*, *23*(4), 1004–1013.
- 358 Baisya, H., & Pattnaik, S. (2019). Orographic effect and multiscale interactions during an
 359 extreme rainfall event. *Environmental Research Communications*, *1*(5), 051002.
- 360 Bartels, D. L., Brown, J. M., & Tollerud, E. I. (1997). Structure of a midtropospheric vortex
 361 induced by a mesoscale convective system. *Monthly weather review*, *125*(2), 193–211.
- 362 Bartels, D. L., & Maddox, R. A. (1991). Midlevel cyclonic vortices generated by mesoscale
 363 convective systems. *Monthly Weather Review*, *119*(1), 104–118.
- 364 Boos, W., Hurley, J., & Murthy, V. (2015). Adiabatic westward drift of indian monsoon
 365 depressions. *Quarterly Journal of the Royal Meteorological Society*, *141*(689), 1035–
 366 1048.
- 367 Bosart, L. F., & Sanders, F. (1981). The johnstown flood of july 1977: A long-lived
 368 convective system. *Journal of the Atmospheric Sciences*, *38*(8), 1616–1642.
- 369 Bretherton, C. S., Peters, M. E., & Back, L. E. (2004). Relationships between water vapor
 370 path and precipitation over the tropical oceans. *Journal of climate*, *17*(7), 1517–1528.
- 371 Carlowicz, M. (2019). *Heavy monsoon rains flood south asia*. Retrieved from
 372 [https://earthobservatory.nasa.gov/images/145460/heavy-monsoon-rains](https://earthobservatory.nasa.gov/images/145460/heavy-monsoon-rains-flood-south-asia)
 373 [-flood-south-asia](https://earthobservatory.nasa.gov/images/145460/heavy-monsoon-rains-flood-south-asia)
- 374 Carr, F. H. (1977). Mid-tropospheric cyclones of the summer monsoon. *pure and applied*
 375 *geophysics*, *115*(5-6), 1383–1412.
- 376 Chakraborty, A. (2016). A synoptic-scale perspective of heavy rainfall over chennai in
 377 november 2015. *Current Science (00113891)*, *111*(1).
- 378 Coumou, D., & Rahmstorf, S. (2012). A decade of weather extremes. *Nature climate change*,
 379 *2*(7), 491.
- 380 Dash, S., Kumar, J. R., & Shekhar, M. (2004). On the decreasing frequency of monsoon
 381 depressions over the indian region. *Current Science*, 1404–1411.
- 382 Dee, D. P., Uppala, S. M., Simmons, A. J., Berrisford, P., Poli, P., Kobayashi, S., ...
 383 Vitart, F. (2011, Apr). The ERA-Interim reanalysis: configuration and performance
 384 of the data assimilation system. *Quarterly Journal of the Royal Meteorological Society*,
 385 *137*(656), 553–597.
- 386 Doswell III, C. A., Brooks, H. E., & Maddox, R. A. (1996). Flash flood forecasting: An
 387 ingredients-based methodology. *Weather and Forecasting*, *11*(4), 560–581.
- 388 Emori, S., & Brown, S. (2005). Dynamic and thermodynamic changes in mean and extreme
 389 precipitation under changed climate. *Geophysical Research Letters*, *32*(17).
- 390 Falcão, A. X., Stolfi, J., & de Alencar Lotufo, R. (2004). The image foresting transform:
 391 Theory, algorithms, and applications. *IEEE transactions on pattern analysis and*
 392 *machine intelligence*, *26*(1), 19–29.
- 393 Findlater, J. (1969). A major low-level air current near the indian ocean during the northern
 394 summer. *Quarterly Journal of the Royal Meteorological Society*, *95*(404), 362–380.
- 395 Francis, P., & Gadgil, S. (2006). Intense rainfall events over the west coast of india.
 396 *Meteorology and Atmospheric Physics*, *94*(1-4), 27–42.
- 397 Fritsch, J., Murphy, J., & Kain, J. (1994). Warm core vortex amplification over land.
 398 *Journal of the atmospheric sciences*, *51*(13), 1780–1807.
- 399 George, P. (1956). Effect of off-shore vortices on rainfall along the west coast of india.
 400 *Indian J. Meteorol. Geophys*, *7*, 225–240.
- 401 Godbole, R. V. (1977). The composite structure of the monsoon depression. *Tellus*, *29*(1),
 402 25–40.
- 403 Goswami, B., Ajayamohan, R., Xavier, P. K., & Sengupta, D. (2003). Clustering of synoptic
 404 activity by indian summer monsoon intraseasonal oscillations. *Geophysical Research*
 405 *Letters*, *30*(8).
- 406 Goswami, B. N., Venugopal, V., Sengupta, D., Madhusoodanan, M., & Xavier, P. K. (2006).
 407 Increasing trend of extreme rain events over India in a warming environment. *Science*,
 408 *314*(5804), 1442–1445.
- 409 Hodges, K. (1995). Feature tracking on the unit sphere. *Monthly Weather Review*, *123*(12),
 410 3458–3465.

- 411 Hodges, K. (1999). Adaptive constraints for feature tracking. *Monthly Weather Review*,
412 *127*(6), 1362–1373.
- 413 Holloway, C. E., & Neelin, J. D. (2009). Moisture vertical structure, column water vapor,
414 and tropical deep convection. *Journal of the atmospheric sciences*, *66*(6), 1665–1683.
- 415 Houze Jr, R., McMurdie, L., Rasmussen, K., Kumar, A., & Chaplin, M. (2017). Multiscale
416 aspects of the storm producing the june 2013 flooding in uttarakhand, india. *Monthly*
417 *Weather Review*, *145*(11), 4447–4466.
- 418 Hunt, K. M., & Fletcher, J. K. (2019). The relationship between indian monsoon rainfall
419 and low-pressure systems. *Climate Dynamics*, 1–13.
- 420 Hurley, J. V., & Boos, W. R. (2015). A global climatology of monsoon low-pressure systems.
421 *Quarterly Journal of the Royal Meteorological Society*, *141*(689), 1049–1064.
- 422 Joseph, P., & Sijikumar, S. (2004). Intraseasonal variability of the low-level jet stream of
423 the asian summer monsoon. *Journal of Climate*, *17*(7), 1449–1458.
- 424 Karmakar, N., Chakraborty, A., & Nanjundiah, R. S. (2015). Decreasing intensity of
425 monsoon low-frequency intraseasonal variability over india. *Environmental Research*
426 *Letters*, *10*(5), 054018.
- 427 Karmakar, N., Chakraborty, A., & Nanjundiah, R. S. (2017). Increased sporadic extremes
428 decrease the intraseasonal variability in the Indian summer monsoon rainfall. *Scientific*
429 *reports*, *7*(1), 7824.
- 430 Knievel, J. C., & Johnson, R. H. (2002). The kinematics of a midlatitude, continental
431 mesoscale convective system and its mesoscale vortex. *Monthly weather review*, *130*(7),
432 1749–1770.
- 433 Knievel, J. C., & Johnson, R. H. (2003). A scale-discriminating vorticity budget for a
434 mesoscale vortex in a midlatitude, continental mesoscale convective system. *Journal*
435 *of the atmospheric sciences*, *60*(6), 781–794.
- 436 Krishnamurthy, V., & Ajayamohan, R. (2010). Composite structure of monsoon low pressure
437 systems and its relation to indian rainfall. *Journal of Climate*, *23*(16), 4285–4305.
- 438 Krishnamurti, T., & Hawkins, R. (1970). Mid-tropospheric cyclones of the southwest
439 monsoon. *Journal of Applied Meteorology*, *9*(3), 442–458.
- 440 Krishnamurti, T., Kanamitsu, M., Godbole, R., Chang, C., Carr, F., & Chow, J. (1975).
441 Study of a monsoon depression (i): Synoptic structure. *J. Meteor. Soc. Japan*, *53*,
442 227–239.
- 443 Kumar, A., Dudhia, J., Rotunno, R., Niyogi, D., & Mohanty, U. (2008). Analysis of
444 the 26 july 2005 heavy rain event over mumbai, india using the weather research
445 and forecasting (wrf) model. *Quarterly Journal of the Royal Meteorological Society*,
446 *134*(636), 1897–1910.
- 447 Maddox, R. A., Chappell, C. F., & Hoxit, L. R. (1979). Synoptic and meso- α scale aspects
448 of flash flood events. *Bulletin of the American Meteorological Society*, *60*(2), 115–123.
- 449 Maddox, R. A., Hoxit, L. R., Chappell, C. F., & Caracena, F. (1978). Comparison of me-
450 teorological aspects of the big thompson and rapid city flash floods. *Monthly Weather*
451 *Review*, *106*(3), 375–389.
- 452 Miller, F. R., & Keshavamurthy, R. (1968). *Structure of an arabian sea summer monsoon*
453 *system*. Univ of Hawaii Pr.
- 454 Muller, C. J., O’Gorman, P. A., & Back, L. E. (2011). Intensification of precipitation
455 extremes with warming in a cloud-resolving model. *Journal of Climate*, *24*(11), 2784–
456 2800.
- 457 Murakami, T., Nakazawa, T., & He, J. (1984). On the 40-50 day oscillations during the
458 1979 northern hemisphere summer. *Journal of the Meteorological Society of Japan*.
459 *Ser. II*, *62*(3), 440–468.
- 460 Nikumbh, A. C., Chakraborty, A., & Bhat, G. (2019). Recent spatial aggregation tendency
461 of rainfall extremes over india. *Scientific reports*, *9*(1), 10321.
- 462 O’Gorman, P. A. (2015). Precipitation extremes under climate change. *Current climate*
463 *change reports*, *1*(2), 49–59.
- 464 Phadtare, J. (2018). Role of eastern ghats orography and cold pool in an extreme rainfall
465 event over chennai on 1 december 2015. *Monthly Weather Review*, *146*(4), 943–965.

- 466 Phadtare, J., & Bhat, G. (2019). Characteristics of deep cloud systems under weak and
 467 strong synoptic forcing during the indian summer monsoon season. *Monthly Weather*
 468 *Review*, *147*(10), 3741–3758.
- 469 Pradhan, P., Dasamsetti, S., Ramakrishna, S., Dodla, V., & Panda, J. (2015). Mesoscale
 470 simulation of off-shore trough and mid-tropospheric cyclone associated with heavy
 471 rainfall along the west coast of india using armex reanalysis. *International Journal of*
 472 *Earth and Atmospheric Science*, *2*(1), 01–15.
- 473 Rajeevan, M., Bhate, J., & Jaswal, A. K. (2008). Analysis of variability and trends of
 474 extreme rainfall events over india using 104 years of gridded daily rainfall data. *Geo-*
 475 *physical Research Letters*, *35*(18), L18707.
- 476 Rajeevan, M., Bhate, J., Kale, J., & Lal, B. (2006). High resolution daily gridded rainfall
 477 data for the indian region: Analysis of break and active. *Current Science*, *91*(3),
 478 296–306.
- 479 Rao, K., & Rajamani, S. (1970). Diagnostic study of a monsoon depression by geostrophic
 480 baroclinic model. *Indian Journal of Meteorology and Geophysics*, *21*, 187–194.
- 481 Rao, Y. (1976). Southwest monsoon. *Meteorological monograph synoptic meteorology*, *1*,
 482 2.2.
- 483 Rasmussen, K. L., & Houze Jr, R. A. (2012). A flash-flooding storm at the steep edge
 484 of high terrain: disaster in the himalayans. *Bulletin of the American Meteorological*
 485 *Society*, *93*(11), 1713–1724.
- 486 Raymond, D., & Jiang, H. (1990). A theory for long-lived mesoscale convective systems.
 487 *Journal of the atmospheric sciences*, *47*(24), 3067–3077.
- 488 Sanders, F. (1984). Quasi-geostrophic diagnosis of the monsoon depression of 5–8 july 1979.
 489 *Journal of the Atmospheric Sciences*, *41*(4), 538–552.
- 490 Schumacher, R. S., & Johnson, R. H. (2005). Organization and environmental properties
 491 of extreme-rain-producing mesoscale convective systems. *Monthly weather review*,
 492 *133*(4), 961–976.
- 493 Schumacher, R. S., & Johnson, R. H. (2009). Quasi-stationary, extreme-rain-producing
 494 convective systems associated with midlevel cyclonic circulations. *Weather and Fore-*
 495 *casting*, *24*(2), 555–574.
- 496 Sikka, D. (1977). Some aspects of the life history, structure and movement of monsoon
 497 depressions. *pure and applied geophysics*, *115*(5), 1501–1529.
- 498 Sikka, D. (1978). Some aspects of the life history, structure and movement of monsoon
 499 depressions. In *Monsoon dynamics* (pp. 1501–1529). Springer.
- 500 Sutcliffe, R. (1947). A contribution to the problem of development. *Quarterly Journal of*
 501 *the Royal Meteorological Society*, *73*(317-318), 370–383.
- 502 Thiruppugazh, V. (2019). *Gujarat flood 2017 case study*. Retrieved from [https://ndma](https://ndma.gov.in/images/guidelines/gujrat-flood-study-2017.pdf)
 503 [.gov.in/images/guidelines/gujrat-flood-study-2017.pdf](https://ndma.gov.in/images/guidelines/gujrat-flood-study-2017.pdf)
- 504 Trenberth, K. E. (1978). On the interpretation of the diagnostic quasi-geostrophic omega
 505 equation. *Monthly Weather Review*, *106*(1), 131–137.
- 506 Trenberth, K. E. (1999, May 01). Conceptual framework for changes of extremes of the
 507 hydrological cycle with climate change. *Climatic Change*, *42*(1), 327–339.
- 508 Vishnu, S., Francis, P., Shenoi, S., & Ramakrishna, S. (2016). On the decreasing trend
 509 of the number of monsoon depressions in the bay of bengal. *Environmental Research*
 510 *Letters*, *11*(1), 014011.
- 511 Wang, B. (2006). *The asian monsoon*. Springer Science & Business Media.

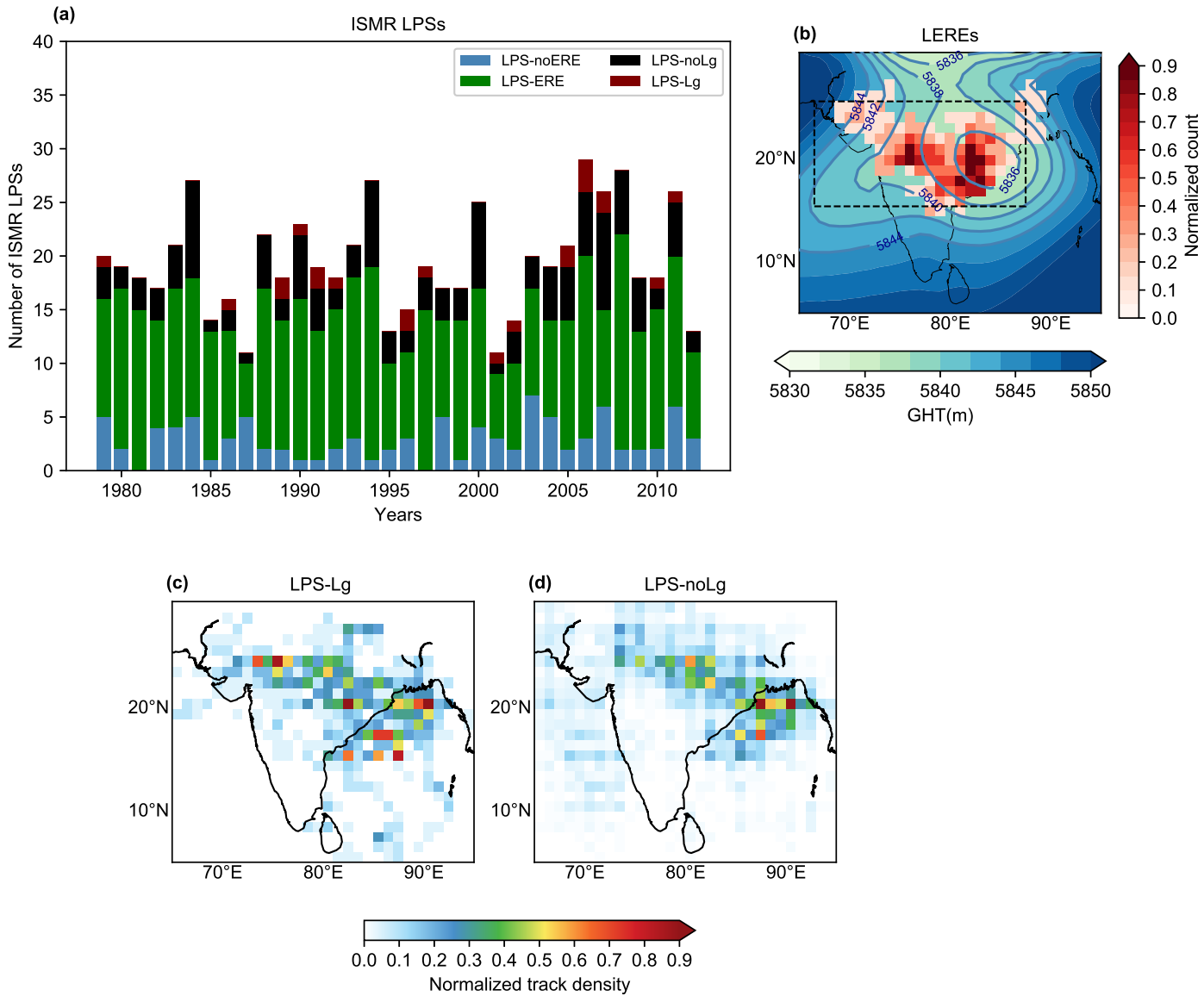


Figure 1. (a) Seasonal counts of monsoon low pressure systems (LPSs) that lead to extreme rainfall events (LPS-ERE), LPSs that did not lead to an ERE (LPS-noERE), LPSs that lead to LEREs (LPS-Lg), strong LPSs (intensity ≥ 2) that did not cause LEREs (LPS-noLg) observed during the study period (1979-2012). (b) Spatial distribution of LEREs and the JJAS climatology of geopotential height at 500 hPa. The count of LEREs is normalized by the maximum count over the study region ($15^{\circ} - 25^{\circ}\text{N}$, $65^{\circ} - 85^{\circ}\text{E}$). Track density of (c) LPS-Lg and (d) LPS-noLg. The track density is the number of tracks of LPSs per grid and is normalized with respect to the maximum value over the region ($0^{\circ} - 30^{\circ}\text{N}$, $60^{\circ} - 90^{\circ}\text{E}$). The dotted inset box in Fig 1b. represents the study region ($15^{\circ} - 25^{\circ}\text{N}$, $65^{\circ} - 85^{\circ}\text{E}$).

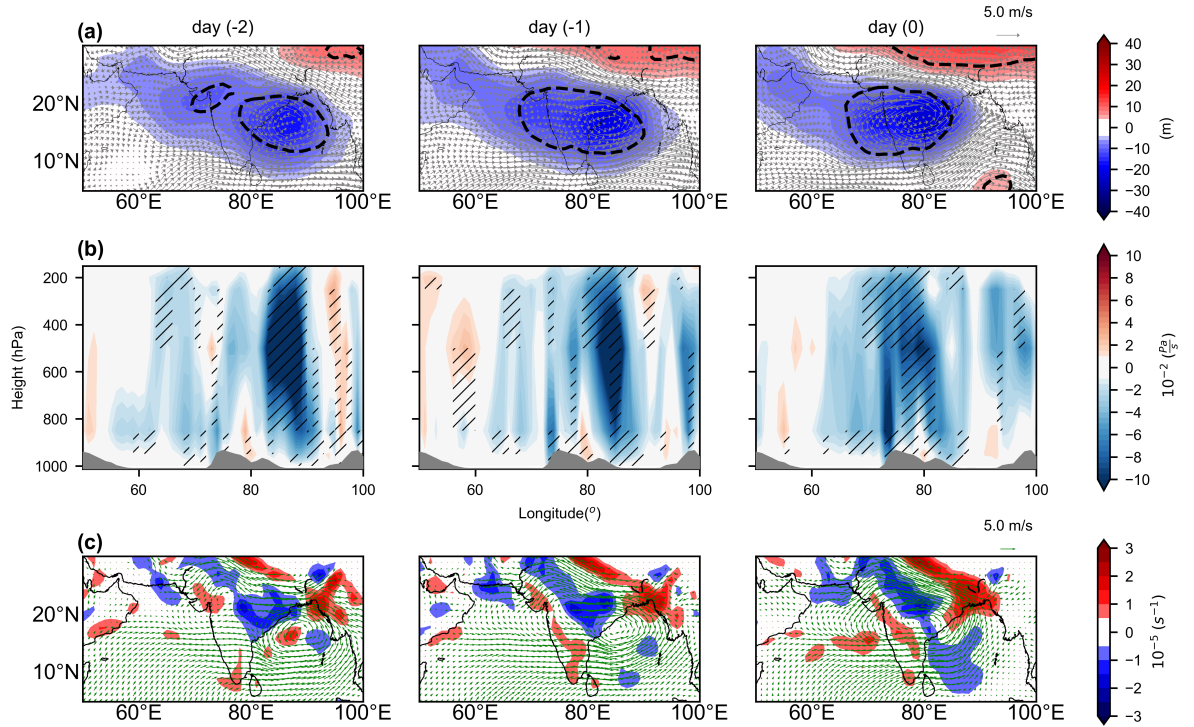


Figure 2. Lagged composites of anomalous (a) geopotential height (m), wind ($\frac{m}{s}$) at 500 hPa, (b) pressure velocity ($\frac{Pa}{s}$), and (c) wind divergence (s^{-1}), wind ($\frac{m}{s}$) at 850 hPa for LPS-Lg from day(-2) to day(0) (left to right). Day-0 indicates the day of LERE. The pressure velocity is meridionally averaged from 15° to 25°N. The dotted contour and hatching represent statistically significant anomalies for geopotential height (t-test: p -value < 0.01) and pressure velocity (t-test: p -value < 0.05), respectively.

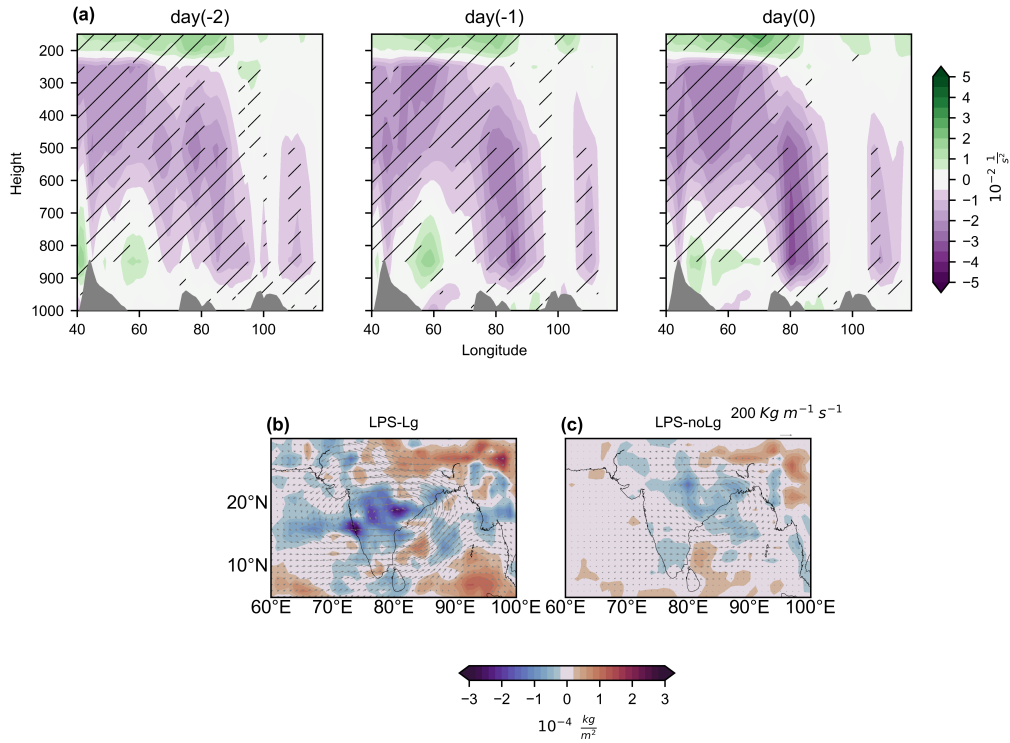


Figure 3. (a) Lagged composite of static stability anomalies for LPS-Lg from lag day(-2) to day(0). The anomalies are meridionally averaged from 15° to 25° N. The hatching represents statistically significant anomalies (t-test: p - value < 0.05). Composite vertically integrated moisture divergence (shading) and moisture transport (vectors) anomalies for (b)LPS-Lg on the LERE day and for (c)LPS-noLg at the middle location of the LPS track.

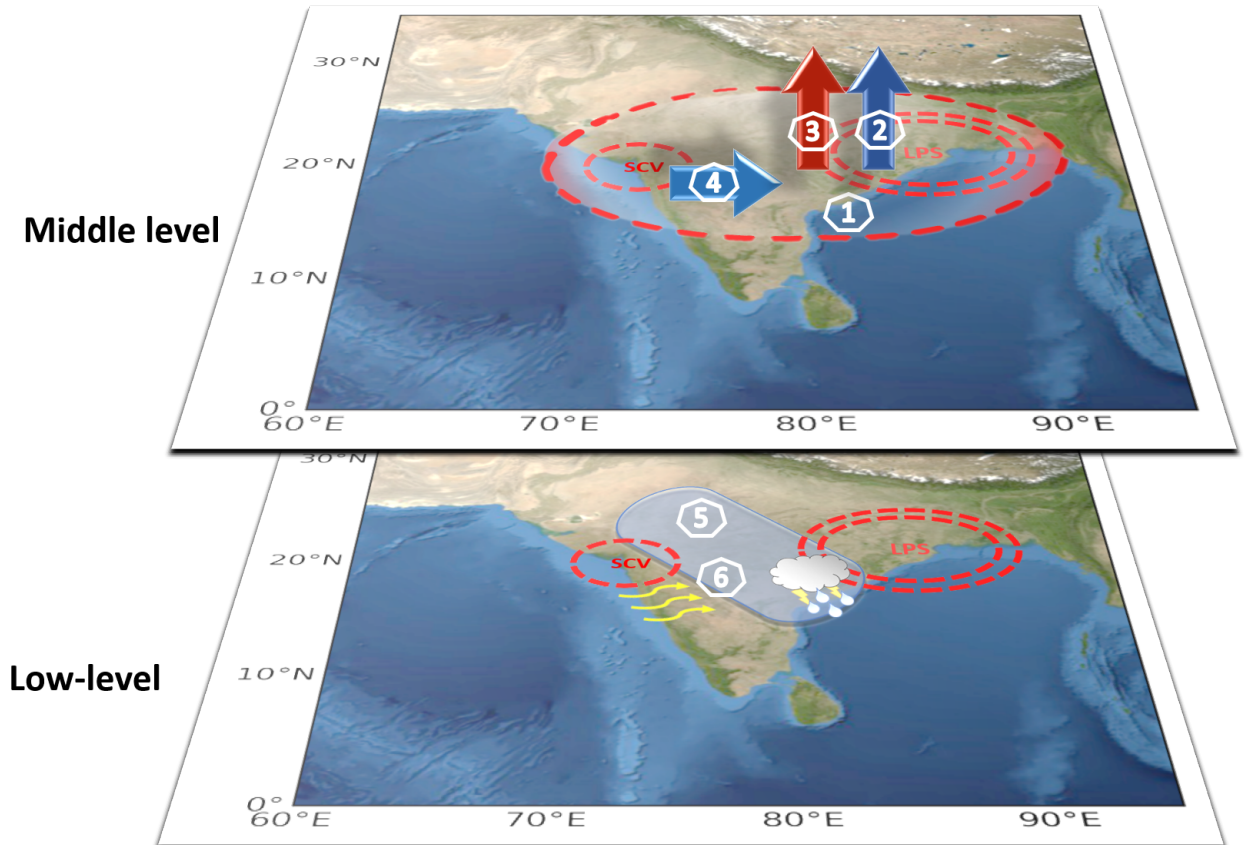


Figure 4. Schematic explaining the mechanism of LEREs. The interaction of an LPS and an SCV forms conditions favourable for long-lived, organized and slow moving convective systems on the western flank of the LPS, which result in LEREs. The numbers from 1 to 6 in the figure are representative of terms viz., mid-tropospheric vortex, dynamic lifting, static instability, moisture supply, an organization at the low-level, and LPS translation speed, respectively. These terms are explained in the summary section.

Figure 1.

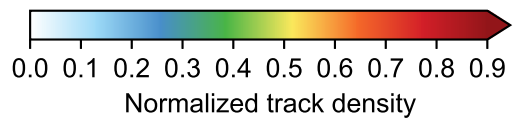
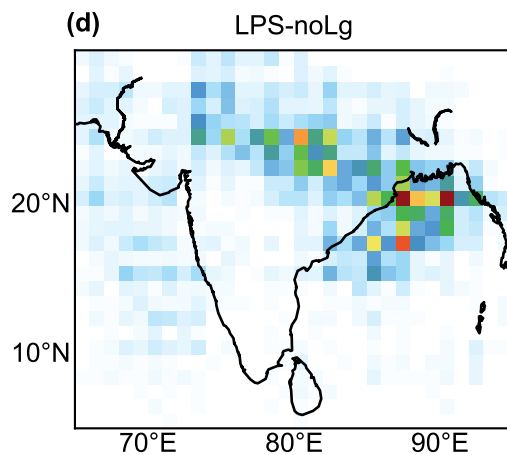
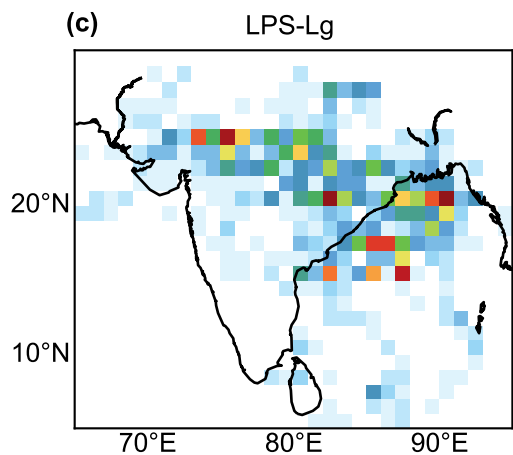
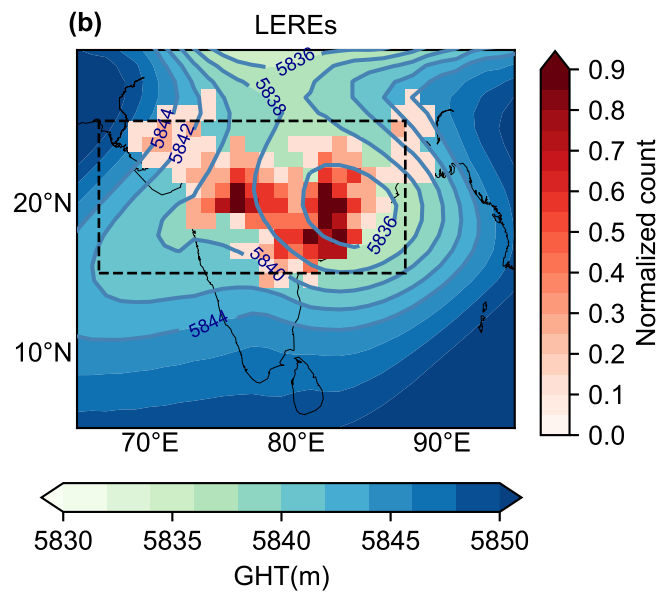
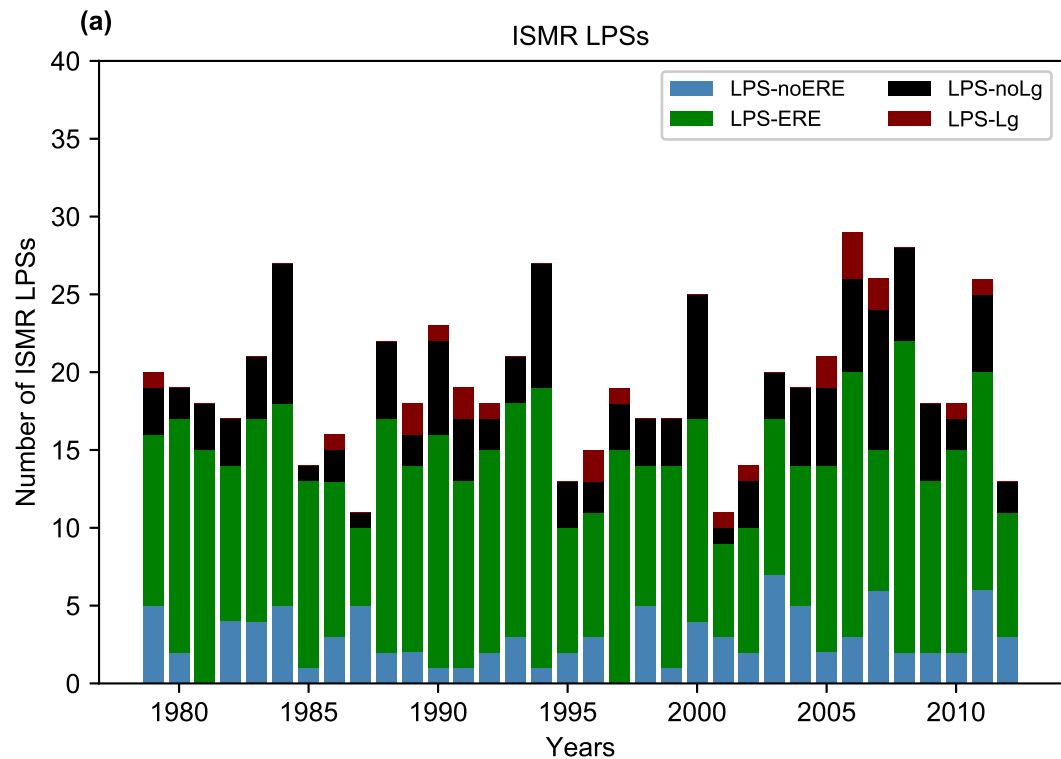


Figure 2.

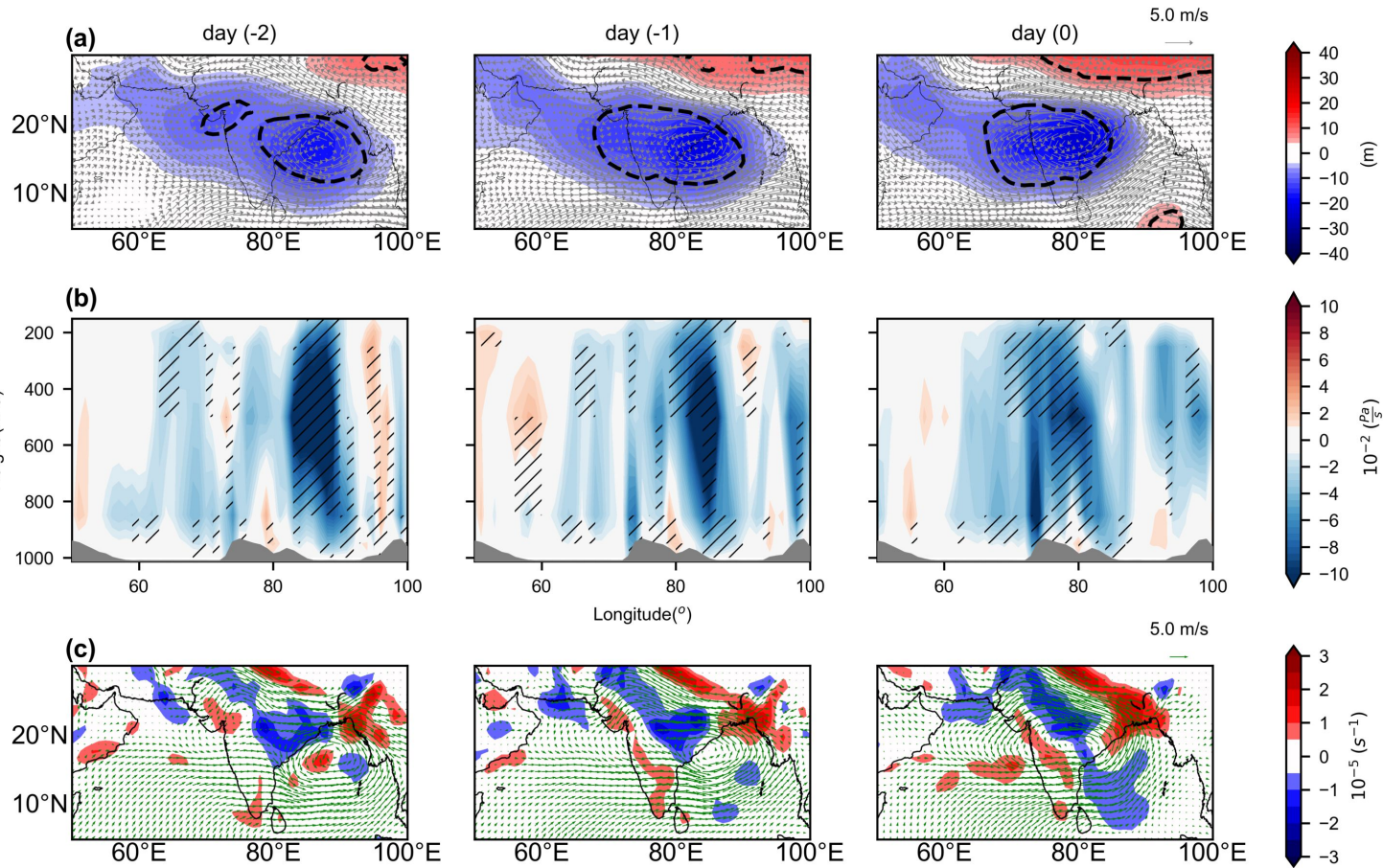


Figure 3.

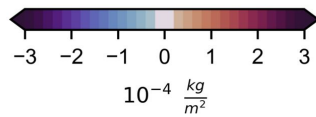
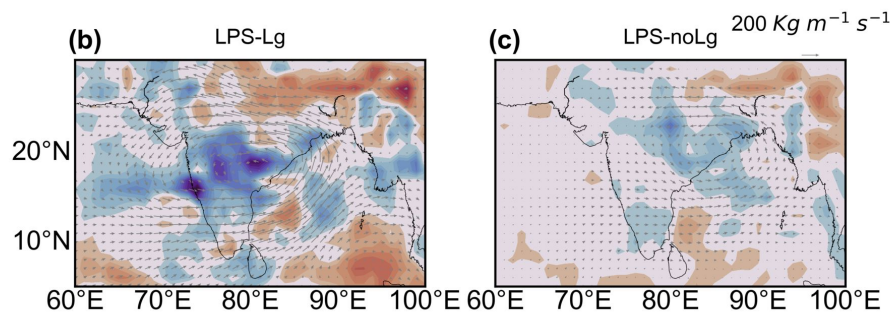
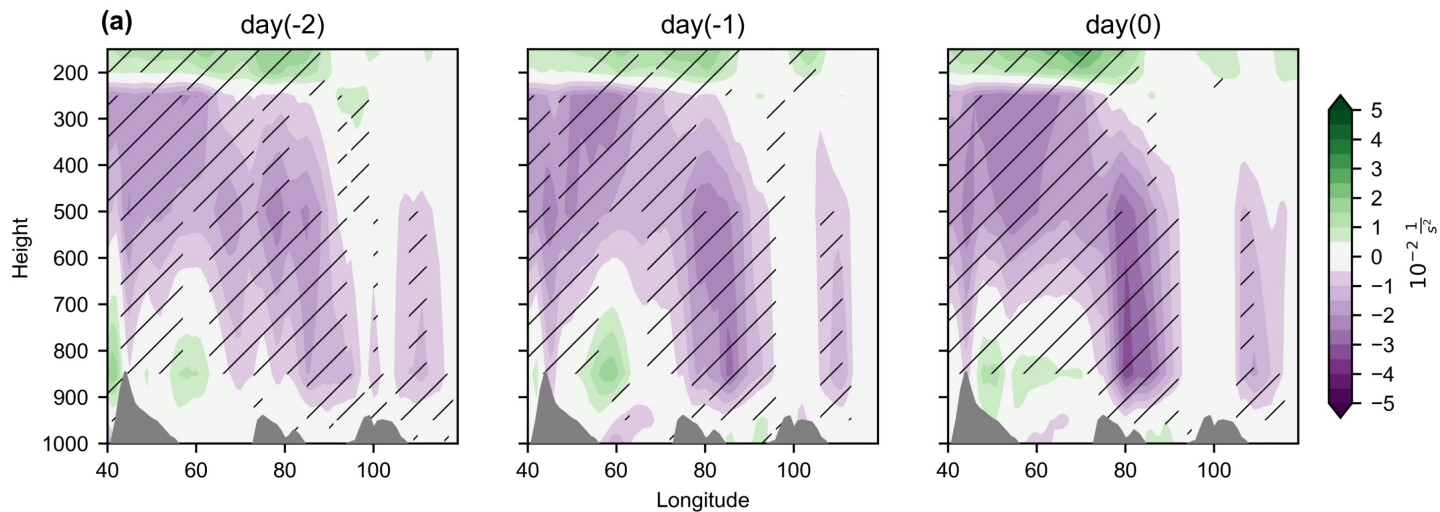
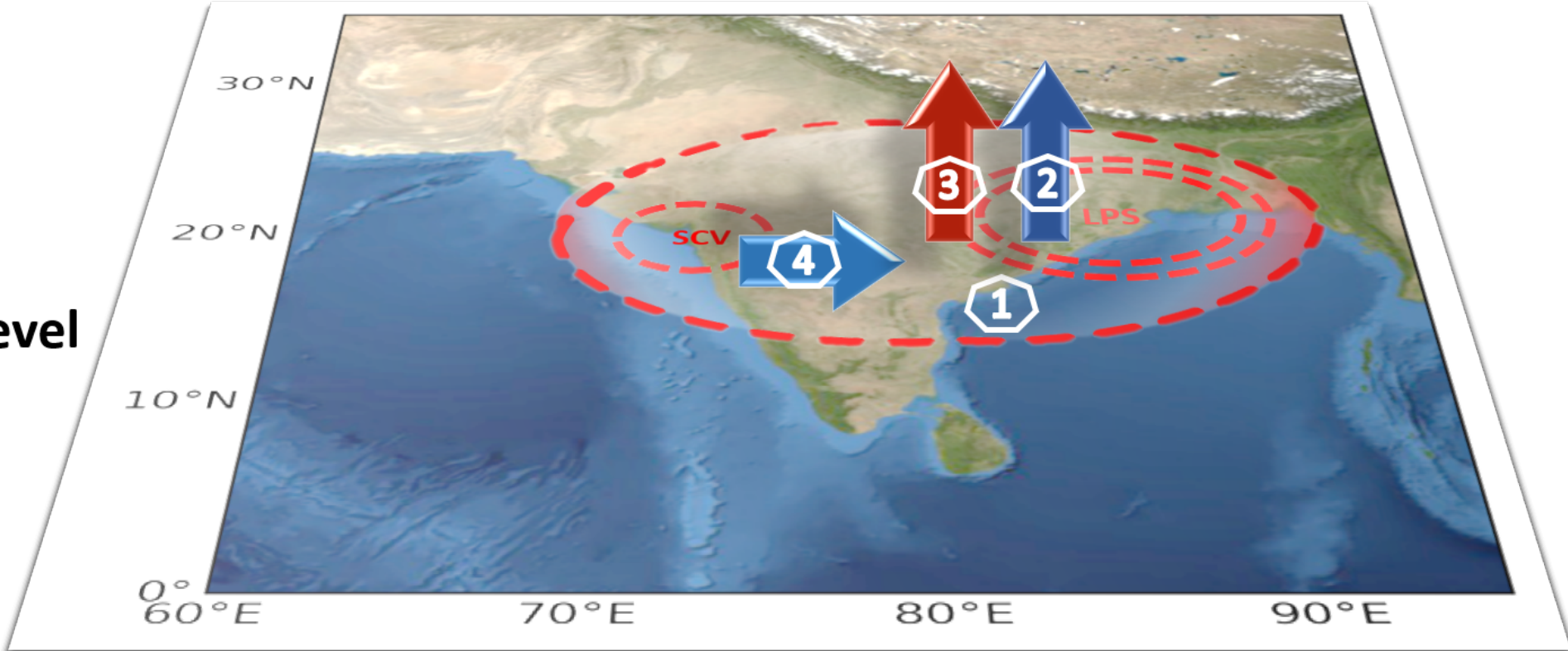


Figure 4.

Middle level



Low-level

